Acta Biomaterialia xxx (xxxx) xxx

Contents lists available at ScienceDirect

Acta Biomaterialia

journal homepage: www.elsevier.com/locate/actabiomat

Full length article

Osteomimetic matrix components alter cell migration and drug response in a 3D tumour-engineered osteosarcoma model

M. Pavlou [a,b], M. Shah [a], P. Gikas [c], T. Briggs [c], S.J. Roberts [a,d,1], U. Cheema [a,1,*]

[a] UCL Institute of Orthopaedics and Musculoskeletal Sciences, UCL Division of Surgery and Interventional Science, RNOH Campus, Stanmore, HA7 4LP, UK
[b] Department of Pharmacy, Faculty of Chemistry and Pharmacy, Ludwig-Maximilians University Munich, Butenandstr. 5-13, Munich 81377, Germany
[c] Royal National Orthopaedic Hospital, Stanmore, HA7 4LP, UK
[d] Department of Comparative Biomedical Sciences, The Royal Veterinary College, London, NW1 0TU, UK

ARTICLE INFO

Article history:
Received 30 January 2019
Received in revised form 10 June 2019
Accepted 9 July 2019
Available online xxxx

Keywords:
3D model
Tumour engineering
Osteosarcoma niche
Biomimetic
Doxorubicin

ABSTRACT

Osteosarcoma management continues to lack the appropriate prognostic tools to assign personalised treatment. This leaves non-responders to standard care vulnerable to recurring disease and pulmonary metastases. Developing 3D *in vitro* disease models to serve as a test bed for personalised treatment is a promising approach to address this issue. This study describes the generation of 3D osteosarcoma models termed "tumouroids", which are geometrically compartmentalised to reproduce the bone cancer mass and its surrounding. Although the tumour microenvironment impacts osteosarcoma in many ways, this model focussed on interrogating the influence of a biomimetic matrix on tumour cell behaviour. The 3D matrix was supplemented with the bone-marrow proteins laminin, fibronectin and NuOss® bone granules. This led to increased invasion of osteosarcoma cell aggregates from within the bone-like matrix into the surrounding acellular bone marrow-like ECM. The presence of bone granules also yielded an atypical molecular profile of osteosarcoma cells, suggesting malignant metabolic reprogramming. Changes include decreased *MMP-9* ($p < 0.05$) and increased *PTEN* ($p < 0.05$), *MCP-1* ($p < 0.01$) and *MCT-4* ($p < 0.05$) gene expression. This complex 3D biomimetic composition also changed cellular responses to doxorubicin, a common chemotherapeutic agent used to treat osteosarcoma, and reproduced key issues of *in vivo* treatment like drug penetrance and doxorubicin-induced bone toxicity. This work highlights the importance of a biomimetic matrix in 3D osteosarcoma models for both basic and translational research.

Statement of Significance

This study describes the generation of 3D osteosarcoma models termed "tumouroids", which are geometrically compartmentalised to reproduce the bone cancer mass and its environment. Utilising this novel model, specific parameters of osteosarcoma growth and invasion were investigated. Osteosarcoma cell lines proliferate at a slower rate, exhibit malignant metabolic reprogramming, and respond to drug intervention at lower concentrations of doxorubicin hydrochloride in matrix-complex compared to basic tumouroids. As such, this study provides evidence that the tumour microenvironment impacts osteosarcoma in many ways. The osteosarcoma tumouroid described herein may form the basis of a personalised-medicine strategy, which will allow the testing of drug effectiveness similar to that used for antibiotic selection for pathogenic bacteria.

1. Introduction

Many cancer patients will obtain little benefit from existing anti-cancer treatments. This is particularly true for patients with rare and highly heterogeneous cancers, such as osteosarcoma. Osteosarcoma is the most common solid tumour of bones occurring predominantly within the metaphyseal medullary cavity of long bones, with high-grade intramedullary osteoblastic osteosarcoma the most commonly diagnosed subtype [1]. There is a growing body of evidence to suggest that mesenchymal stem cells and their osteoblastic lineage are the cells-of-origin resulting in this cancer [2]. Therapeutic efficacy is defined by the Huvos grading

* Corresponding author.
E-mail address: u.cheema@ucl.ac.uk (U. Cheema).
[1] Shared Senior Authorship.

https://doi.org/10.1016/j.actbio.2019.07.011
1742-7061/

Please cite this article as: M. Pavlou, M. Shah, P. Gikas et al., Osteomimetic matrix components alter cell migration and drug response in a 3D tumour-engineered osteosarcoma model, Acta Biomaterialia, https://doi.org/10.1016/j.actbio.2019.07.011

system of tumour necrosis following chemotherapy and surgical excision, where good responders are termed those above the 90% threshold and poor responders those below. However, this prognostic system offers no insight on how to manage poor responders. As such, there is an urgent need for an osteosarcoma personalised-medicine modality. Whilst basic research advances our understanding of disease mechanisms and informs on potential drugable signalling nodes, it stops short of informing clinicians about treatment alternatives.

There is a growing appreciation of the importance of the microenvironment and niche to the properties of cancer cells. Like their healthy counterparts, cancer cells exist in a dynamic 3D environment mediated by cell-to-cell and cell-to-extracellular matrix (ECM) interactions. Cells types within the microenvironment include osteoblasts, osteoclasts, pericytes and (other vascular cells) and cells of the haematopoietic lineage [2]. The physical niche includes the bone, both trabecular and cortical, and the bone marrow. These physical environments confer different matrix compositions, matrix architecture, oxygen levels and stiffness. Bone is a highly vascular tissue, with a hard, mineralised matrix, mainly composed of collagen and hydroxyapatite conferring a young's modulus of 15.2 GPa [3]. In comparison, bone marrow and marrow adipose tissue are composed of collagen, fibronectin, laminin, proteoglycans and hyaluronan, and a number of minor components (Fig. 1) [4]. The young's modulus of bone marrow varies between 0.25 and 15.7 kPa [5] and is thus much less stiff than bone. Appreciation of the difference in characteristics of the bone and bone marrow is essential when aiming to replicate *in vivo* biology with an *in vitro* model of the disease. Indeed, bone density [6,7], platelet-assisted intravasation [8–10], hypoxia [11,12] and matrix composition [13,14] are all mediators of osteosarcoma development. The research presented herein focuses on the role of the matrix composition in the osteosarcoma niche on cancer cell behaviour.

Through the adoption of established tissue engineering tools, a new generation of 3D *in vitro* cancer models can be created via tumour engineering. Herein we report the development of 'tumouroids' as a novel 3D *in vitro* model of osteosarcoma. The aim of this study is to create a customisable system that would allow the interrogation of the influence of the ECM on osteosarcoma drug sensitivity. Specifically, it aims to understand how non-cellular components of the tumour mass and matrix, namely ECM proteins, change invasion of cancer and response to a therapeutic insult. The 'tumouroids' are based on the matrix protein collagen type I and have a geometrically modular 3D structure. This compartmentalisation allows the composition of each module to be varied in order to best represent the cancer mass and the organic and inorganic features of its surrounding stroma (Fig. 1). Due to the transparency of these cultures it is possible to track the migration/invasion of cancer cells into the surrounding ECM as well as any changes in cancer mass morphology. The modulation of the matrix composition of individual tumouroid compartments had an impact on the morphological and molecular profile of cancer cells, which was also reflected in the drug response to doxorubicin.

2. Materials and methods

2.1. Cell culture

The MG-63 (ATCC® CRL-1427™) and the 143B (ATCC® CRL-8303™) human bone osteosarcoma cell lines were purchased from ATCC. MG-63 and 143B cells were cultured in high-glucose Dulbecco's Modified Eagle Medium (DMEM) (Thermo Fisher Scientific, Paisley, UK) supplemented with 10% fetal bovine serum (FBS) (Gibco, Loughborough, UK), 1% antibiotic-antimyotic solution 100x (Thermo Fisher Scientific, Paisley, UK) and 1% sodium pyruvate 100 mM (Thermo Fisher Scientific, Paisley, UK). Cells were maintained in 37 °C, 5% CO_2/air and 95% humidity. Cells were passaged using TryPLE™ Express (Thermo Fisher Scientific, Paisley, UK) and then either re-plated with a seeding density of $4x10^4$ cells/cm^2 or used directly as cell suspension for 3D tumouroid cultures.

2.2. Fabrication of basic 3D tumouroid cultures

3D tumouroid cultures were generated using a customised protocol of the RAFT™ 3D cell culture system (Lonza, Slough, UK) following the manufacturer's instructions. All reagents and workflow solutions were kept on ice unless otherwise stated. Separate solutions for the cellular artificial cancer mass (ACM) and the

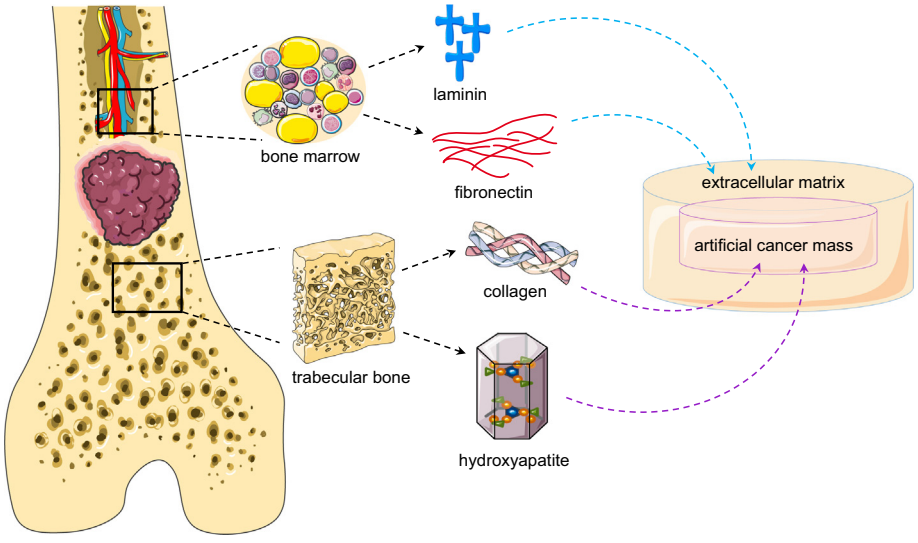

Fig. 1. The extracellular matrix of the osteosarcoma niche modelled in 3D tumouroids. Schematic diagram of the osteosarcoma microenvironment, comprised of the bone-marrow cavity and trabecular bone. The extracellular matrix constituents of each region are annotated, namely laminin, fibronectin, collagen and hydroxyapatite. 3D tumouroids were designed to be geometrically compartmentalised in order to reproduce the matrix composition of the bone-like matrix and the bone-marrow matrix that cancer cells are in contact with. This schematic was generated using elements from the Servier Medical Art database (https://smart.servier.com/).

Please cite this article as: M. Pavlou, M. Shah, P. Gikas et al., Osteomimetic matrix components alter cell migration and drug response in a 3D tumour-engineered osteosarcoma model, Acta Biomaterialia, https://doi.org/10.1016/j.actbio.2019.07.011

surrounding acellular ECM were prepared consecutively. Firstly, the cellular solution; rat-tail collagen type I 2.1 mg/ml in 0.6% acetic acid (First Link, Wolverhampton, UK) was mixed with 10x Minimal Essential Medium (Thermo Fisher Scientific, Paisley, UK) and neutralised to a pH ~ 7 using a 10 M NaOH and HEPES solution. A cell suspension was then added corresponding to 50,000 cells/gel (20.8×10^4 cells/ml). The collagen-MEM-cell solution (8:1:1 ratio) was then cast in 96-well plates (240 μl/well) and placed at 37 °C for 15 min to allow gelation. Subsequently, RAFT™ absorbers (016-1R33) were placed on the hydrogels for 15 min to remove excess fluid and increase collagen density. 200 μl complete media were added over each gel and the 96-well plate was kept briefly at 37 °C, 5% CO_2/air, 95% humidity until the next steps. The acellular ECM solution; collagen was mixed with 10x MEM and neutralised as before, then supplemented with 50 μg/ml laminin (Corning, Amsterdam, Netherlands). The collagen-MEM-laminin solution was cast in 24-well plates (final volume 1.3 ml) and before the solution polymerised, the ACM was transferred from the 96-well plate into the centre of the 24-well plate solution using sterile tweezers. Nested hydrogels were set at 37 °C for 15 min and then compressed using RAFT™ absorbers (016-1R32) for 15 min. This formed the final basic tumouroids (Fig. 2.A.).

2.3. Fabrication of complex 3D tumouroid cultures

Complex 3D tumouroid cultures were prepared using similar methodology as basic, with supplementation of matrix components in the ACM and surrounding ECM. NuOss® cancellous bone granules (0.25–1 mm; Collagen Matrix Inc., Oakland, NJ USA) were grounded under sterile conditions to a particle size < 63 μm in diameter (Ø) using a ceramic pestle and a stainless-steel sieve (510-4901, VWR International Ltd, Lutterworth, UK). As with basic tumouroids, a collagen-MEM-cellular solution was prepared to which 5 mg/ml < 63 μm Ø NuOss® granules were added, mixed and subsequently cast inside 96-well plates. The ACM hydrogels were set at 37 °C for 15 min and then compressed using RAFT™ absorbers (016-1R33) for 5 min. The acellular collagen solution was supplemented with 25 μg/ml laminin and 25 μg/ml fibronectin (Sigma Aldrich) and cast in 24-well plates (final volume 1.3 ml). Before gelation, the ACM was transferred from the 96-well plate into the centre of the 24-well plate solution using sterile tweezers. The nested hydrogels were set at 37 °C for 15 min and then compressed with RAFT™ absorbers (016-1R32) for 10 min. This formed the final complex tumouroids (Fig. 3.A.). All tumouroids were cultured at 37 °C, 5% CO_2/air, 95% humidity in 1 ml/well DMEM and had 50% media change every 48 h.

2.4. Cell proliferation

143B and MG63 basic tumouroids were prepared in triplicates and harvested on Days 0, 3, 5 and 7 to assess proliferation in 3D. 7 days is the standard duration of tumouroid culture in this work unless otherwise stated. Double-strand DNA (dsDNA) quantification was carried out using the Qubit® dsDNA High Sensitivity Assay Kit (Thermo Fisher Scientific) following manufacturer's instructions. Briefly, tumouroids were lysed in RLT buffer (Qiagen) plus 10 μl/ml β-mercaptoethanol (Sigma Aldrich) to avoid interference of phenol-red in TRI Reagent® with the fluorochrome reagent in the Qubit® kit [15]. The lysate was diluted 1/10 in nuclease-free water (Sigma Aldrich). Readings were obtained using the Qubit™ 3.0 Fluorometer and were calculated as total dsDNA [ng/μl] per tumouroid. Growth rates were deduced using the curves of best fit (Fig. 2.H.). Cell proliferation rates of 2D monolayers was also performed using PrestoBlue® Cell Viability Reagent (Thermo Fisher Scientific). A standard curve was deduced on Day 0 which was then used to monitor the proliferation of 50,000 cells on days 1, 2 and 4. Growth rates were deduced using the curves of best fit (Fig. 2.I.).

2.5. Immunofluorescence

Tumouroids were fixed using 10% neutral buffered formalin solution for 30 min at room temperature and then washed with PBS (3 × 1 ml/well). Then tumouroids were incubated in 500 μl 4 μg/ml Phalloidin/PBS solution (P5282, Sigma Aldrich, Dorset, UK) for 45 min at room temperature in the dark. The tumouroids were then washed with PBS 1 ml/well and incubated in 500 μl 5 μg/ml DAPI/PBS solution (D9542, Sigma Aldrich, Dorset, UK) for 15 min at room temperature in the dark. Subsequently, the tumouroids were washed and kept in PBS 1 ml/well until imaged using an Apotome.2 (Carl Zeiss, Oberkochen, Germany). Z-stacks were obtained at 10 μm intervals.

2.6. Characterisation of cell movement in 3D tumouroids

3D tumouroids were intentionally designed to have an acellular ECM compartment surrounding the cellular ACM in order to observe cell migration in response to matrix changes and drug treatment. Two distinct patterns of collective cell migration were recorded either cell sheets or invasive spheroid bodies (Fig. 2.D.). Cell sheets were defined by a disorganised accumulation of cells that gradually extended into the surrounding ECM (Fig. 2.C.). To deduce a qualitative invasion profile of 143B and MG63 tumouroids, the following parameters were monitored at 8 fixed locations on tumouroid circumference (Fig. 2.B.): the maximum distance of cell sheets from the ACM margin, the maximum surface area of invasive spheroid bodies and the total number of invasive spheroid bodies per tumouroid. Experimental repeats per condition n > 2 and technical repeats per experiment n > 4.

2.7. Gene expression analysis

Gene expression analysis was performed in accordance with the MIQE guidelines [16]. Total RNA was isolated from day 7 tumouroids; the control condition was tumouroids in a collagen-only ECM and two test conditions were (1) basic tumouroids in a collagen-laminin [50 μg/ml] ECM and (2) complex tumouroids with added NuOss® [5 mg/ml < 63 μm Ø] in the ACM surrounded by a collagen-laminin [25 μg/ml]-fibronectin [25 μg/ml] ECM. TRI Reagent® (Sigma Aldrich, Dorset, UK) was used following the manufacturer's instructions for phenol/chloroform phase separation. RNA was quantified using a NanoDrop spectrophotometer measuring at 260/280 nm and 1000 ng RNA/sample were reverse transcribed using the High Capacity cDNA Reverse Transcriptase Kit (Thermo Fisher Scientific, Paisley, UK) with the program: 25 °C 10 min, 37 °C 120 min, 85 °C 5 min, 4 °C. Transcribed cDNA was assessed via the CFX96 Touch™ Real-Time PCR (RT-PCR) Detection System (40 cycles) using the iTaq Universal SYBR Green Supermix (Bio-Rad, Hertfordshire, UK). Primers were designed using Primer3Plus and NCBI Primer-BLAST, specific to the *Homo sapien* genes: *PTEN, MMP-9, MCP-1* (also known as *CCL2*), *VEGF-A* and *MCT-4* (Table 1). Relative gene expression was calculated using the $2^{-\Delta C_T}$ method using the reference gene GAPDH, which was ranked first as a reference gene in regard to its stability of expression in sarcomas [17].

2.8. Doxorubicin response assay

Basic and complex 3D tumouroids were cultured for 7 days to allow invasion into surrounding ECM and were then exposed for 24 h to doxorubicin hydrochloride at concentrations 0.1 μM, 1 μM and 10 μM (n = 12 per condition), which corresponds to

Please cite this article as: M. Pavlou, M. Shah, P. Gikas et al., Osteomimetic matrix components alter cell migration and drug response in a 3D tumour-engineered osteosarcoma model, Acta Biomaterialia, https://doi.org/10.1016/j.actbio.2019.07.011

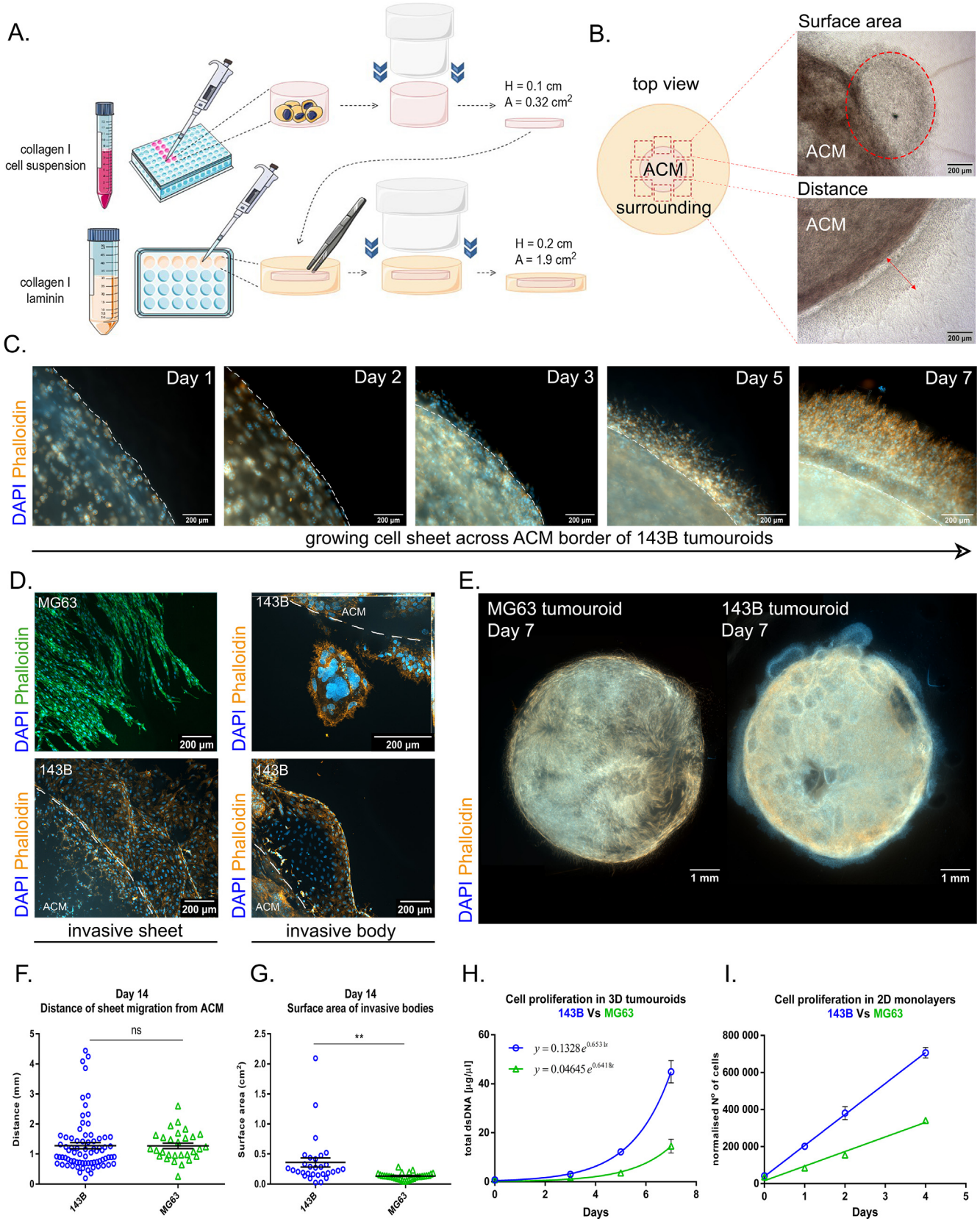

Please cite this article as: M. Pavlou, M. Shah, P. Gikas et al., Osteomimetic matrix components alter cell migration and drug response in a 3D tumour-engineered osteosarcoma model, Acta Biomaterialia, https://doi.org/10.1016/j.actbio.2019.07.011

plasma C_{max} 50–5000 ng/ml. To quantify cell death, tumouroids were processed with the Qubit® dsDNA High Sensitivity Assay Kit, as previously described. To assess metabolic changes, tumouroids were also treated with PrestoBlue® Cell Viability Reagent (Thermo Fisher Scientific) following manufacturer's instructions. This Resazurin-based assay induces changes in Absorbance at 600 nm which were recorded using a Tecan Infinite® 200 PRO plate reader. To observe drug uptake in tumouroids, fluorescence imaging was performed using the Apotome.2 as doxorubicin hydrochloride emits at λ_{em} 595 nm.

2.9. Statistical analysis

Data were collected from biological repeats n > 2 and technical repeats per condition n ≥ 4. The results are presented as mean ± -SEM. Kolmogorov-Smirnov test was performed to compare cumulative distributions and determine whether subsequent analysis required parametric or non-parametric testing. Unpaired Student's *t* test was used to compare two parametric sample populations. For more than two populations, a one-way ANOVA and *post hoc* Tukey's multiple comparisons test was performed and for the drug-response data analysis a two-way ANOVA with *post hoc* Sidak's multiple comparisons test was performed using GraphPad Prism 6. (Graph-Pad, San Diego, CA). The significance level of $\alpha = 0.05$ was accepted. ($p < 0.05$ *, <0.01 **, <0.001 ***).

3. Results

3.1. Highly metastatic 143B cells proliferate faster in basic tumouroids

High-metastatic 143B and low-metastatic MG63 human osteosarcoma cell lines [18] were used to form basic 3D tumouroid cultures. They were defined as 'basic' due to their baseline ECM composition of only collagen type I and laminin (Fig. 2.A.). Viability, proliferation rate and morphological behaviour of cells in 3D was assessed following 7–14 days of culture. Consecutive dsDNA quantification of tumouroids revealed that both cell lines were viable and proliferated exponentially over the 7-day culturing period. A 3-fold higher proliferation rate of 143B compared to MG63 tumouroids was recorded by day 7 (Fig. 2.H.). This is in line with the 2-fold higher proliferation rate of 143B cells compared to MG63 in 2D monolayers (Fig. 2.I.).

3.2. Highly metastatic 143B cells invade as larger spheroid bodies into acellular ECM

3D cell behaviour was monitored daily using brightfield microscopy and fluorescence microscopy measurements. After 7 days of culture it was observed that both cell types in basic tumouroids had migrated from their original seeding location, the ACM, outward into their surrounding acellular ECM (Fig. 2.B & 2.E.). This was apportioned to both cell proliferation and collective cell migration. To confirm that this observation was not a displacement effect of the overgrowing cancer cells, untransformed mesenchymal stem cells (MSCs) were used to populate the ACM and were tracked using the CM-Dil cell-tracker dye (Suppl. Fig. 1.A-B). MSCs were used for this approach because the cell-tracker dye would have been undetected after 24 h in the two OS cell lines due to their high proliferation rate, which is not sufficient time to observe invasion in the surrounding ECM. Following the standard 7 day incubation, MSCs were imaged in the acellular ECM compartment with both faded and intact cell-tracker dye (Suppl. Fig. 1.C-D) thus confirming both migration and proliferation taking place in our 3D culturing system. Two types of collective cell migration were recorded; cell sheets (Fig. 2.B-C.) and spheroid bodies (Fig. 2.B & 2.D.). The former was defined as overlapping cell monolayers with no apparent organisational pattern (Fig. 2.C.) whereas the latter was defined as 3D cellular bodies with a spheroid organisation. Invasive spheroid bodies grew either attached to the circumference of the ACM or detached and migrated into the surrounding ECM (Fig. 2.D.). Due to the 2 types of aggregation and invasion patterns, and the fact that spheroid bodies were not perfect spheres, a measurement of their surface area was selected to define growth. In this 3D model, the formation of invasive spheroid bodies was associated with an aggressive cancer phenotype and the high-metastatic 143B cells, as these developed invasive spheroid bodies of 359.6 ± 75 mm^2 surface area. These were significantly larger than in the low-metastatic MG63 tumouroids which generated invasive spheroid bodies of 133.3 ± 9.7 mm^2 (Fig. 2.G.).

3.3. Addition of matrix components results in enhanced cancer invasion

Complex osteosarcoma tumouroids were so termed due to the addition of matrix components relating to the osteosarcoma niche i.e. the intramedullary cavity, forming a complex ECM. Finely ground < 63 μm Ø cancellous bone granules (NuOss®) were added to the ACM and fibronectin was added to the surrounding ECM compartment of tumouroids (Fig. 3.A.). This triggered both morphological (Fig. 3.B.) and transcriptional changes (Fig. 3.G.) in osteosarcoma cells following 7 days of incubation. The addition of fibronectin in the acellular ECM in the absence of NuOss® had no significant effect on either the distance or surface area of invading cell bodies (Suppl. Fig. 2.A-E.). 143B complex tumouroids produced cell sheets that migrated 1180 ± 117.4 μm from the ACM and 3.7 ± 0.5 invasive bodies per tumouroid, which was significantly greater than their basic counterparts (Fig. 3.C.). MG63 complex tumouroids also showed a trend for increased stromal invasion as they developed cell sheets 800 ± 64.2 μm far from the ACM, however no other parameters showed significant change (Fig. 3.D.).

Fig. 2. Assembly of 3D engineered osteosarcoma tumouroids and behavioural assessment. A. Schematic diagram of basic tumouroid production indicating the requirement for two collagen-based solutions to be prepared which will form the two separate compartments of the final tumouroid. The dimensions of the compressed ACM and compressed final tumouroid are indicated. This schematic was generated using elements from the Servier Medical Art database (https://smart.servier.com/). B. Schematic diagram of the top-down view of tumouroids. The 8 fixed loci where measurements of invasion were performed are marked in red-dotted squares. Representative Brightfield images are shown, indicating how measurements of surface area and distance of invasion were recorded. C. Panel of the chronological aggregation of 143B cells within the ACM by day 2 and the gradual formation of a 3D cell sheet penetrating the acellular surrounding for time points 1, 2, 3, 5 and 7 days. The ACM margin is annotated by a white-dotted line. D. Panel of representative fluorescent images showing examples of the 3D collective cell invasion patterns, cell-sheets and spheroid bodies, formed by MG63 and 143B after 7 days of incubation. E. Birdseye view of MG63 and 143B basic tumouroids after 7 days of incubation. These are collages of single fluorescence images of the ACM compartment of the tumouroids. F. Qualitative assessment of the different rates of cell invasion between 143B and MG63 into a basic ECM surround, in regards to distance of cell-sheets from the ACM margin achieved after 14 days incubation. G. Qualitative assessment of the different rates of cell invasion between 143B and MG63 into a basic ECM surround, in regards to surface area of invasive bodies formed after 14 days incubation. H. Quantitative assessment of cell proliferation of MG63 and 143B cells in a 3D environment with basic ECM composition over a 7 day period, via dsDNA quantification. I. Quantitative assessment of cell proliferation of MG63 and 143B cells in 2D monolayers, using PrestoBlue and a standard curve to deduce the normalised number (No) of cells. ACM = artificial cancer mass; ECM = extracellular matrix; error bars = standard error of mean. (For interpretation of the references to colour in this figure legend, the reader is referred to the web version of this article.)

Please cite this article as: M. Pavlou, M. Shah, P. Gikas et al., Osteomimetic matrix components alter cell migration and drug response in a 3D tumour-engineered osteosarcoma model, Acta Biomaterialia, https://doi.org/10.1016/j.actbio.2019.07.011

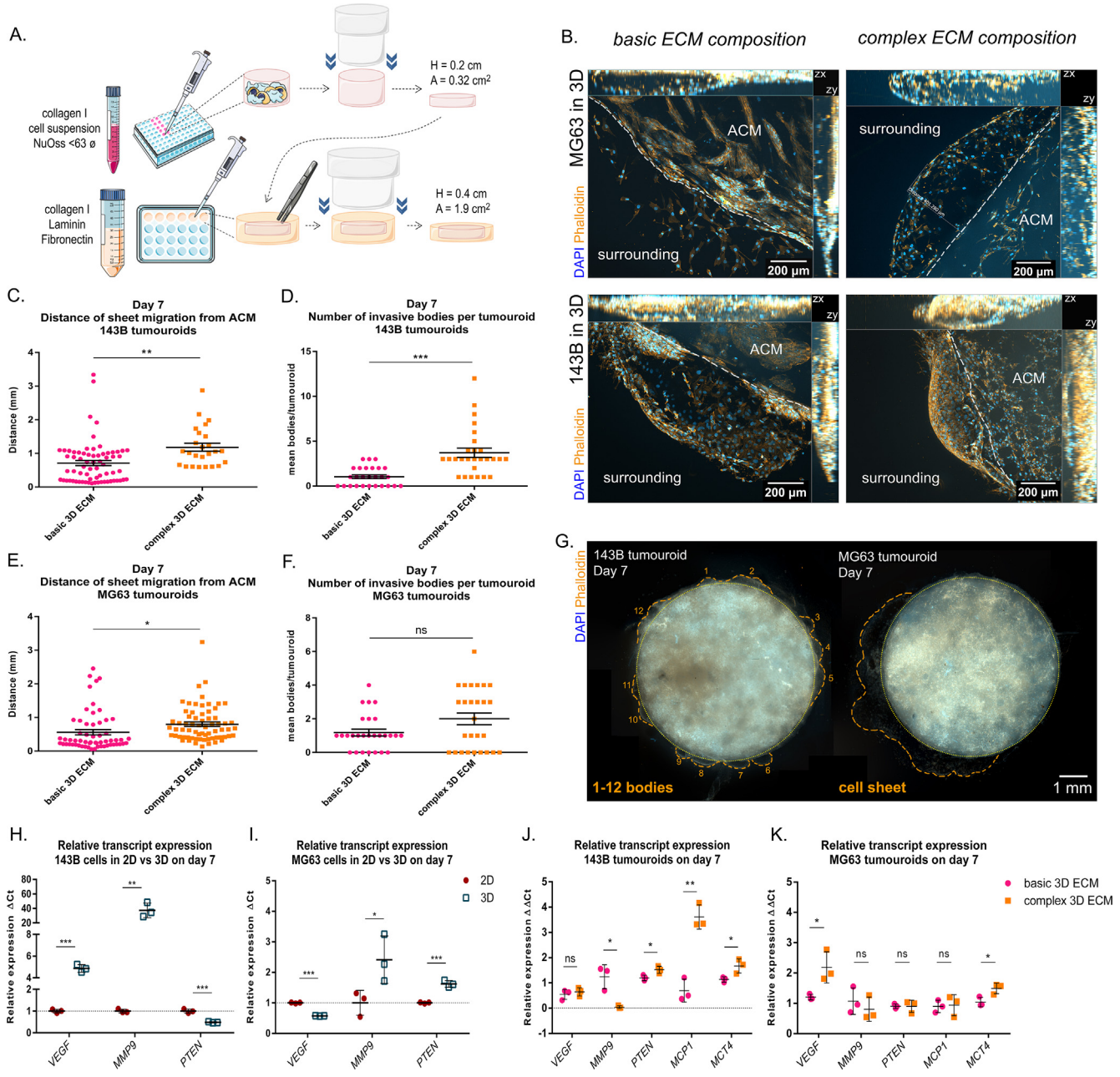

Fig. 3. Formation and characterisation of complex tumouroids. A. Schematic diagram of complex tumouroid production indicating the requirement for two collagen-based solutions to be prepared which will form the two separate compartments of the final tumouroid. The solution used to make the ACM is supplemented with NuOss® granules (<63 µm ø) and the solution used to make the surrounding ECM is supplemented with Fibronectin. The dimensions of the compressed ACM and compressed final tumouroid are disclosed. This schematic was generated using elements from the Servier Medical Art database (https://smart.servier.com/). B. Panel of representative fluorescent images showing examples of morphological modifications occurring to the 3D collective cell invasion patterns depending on the ECM composition of tumouroids. Both MG63 and 143B tumouroids are shown after 7 days of incubation. The ACM margin is indicated by a white dotted line and annotation. C. Effect of basic and complex 3D matrix composition on 143B cell invasion, in regards to distance of cellsheets from ACM margin. D. Effect of basic and complex 3D matrix composition on 143B cell invasion, in terms of invasive bodies per tumouroid. E. Effect of basic and complex 3D matrix composition on MG63 cell invasion, in regards to distance of cellsheets from ACM margin. F. Effect of basic and complex 3D matrix composition on MG63 cell invasion, in terms of invasive bodies per tumouroid. G. Birdseye view of MG63 and 143B complex tumouroids after 7 days of incubation. These are collages of single fluorescence images of the ACM compartment of the tumouroids. For the 143B complex tumouroid the number of invasive bodies are marked with an orange dotted line and numbered. For the MG63 complex tumouroid the periphery of the cell sheet in marked with an orange dotted line. The ACM margin in both tumouroids is indicated by a yellow dotted line. H. Relative changes in transcript levels of selected genes from cells cultured in 2D 143B monolayers compared to 3D collagen after 7 days incubation. Data shown as ΔCt normalised to reference gene *GAPDH*. I. Relative changes in transcript levels of selected genes from cells cultured in 2D MG63 monolayers compared to 3D collagen after 7 days incubation. Data shown as ΔCt normalised to reference gene *GAPDH*. J. Relative changes in transcript levels of selected genes from 143B 3D tumouroids without added NuOss® (basic) and 3D tumouroids with added NuOss® (complex) after 7 days incubation. Data shown as ΔΔCt after first normalising to reference gene *GAPDH* and then to transcript levels obtained from 3D collagen-only tumouroids. (ns = not significant, $p < 0.05$=*, $p < 0.01$=**, $p < 0.001$=***). K. Relative changes in transcript levels of selected genes from MG63 3D tumouroids without added NuOss® (basic) and 3D tumouroids with added NuOss® (complex) after 7 days incubation. Data shown as ΔΔCt after first normalising to reference gene *GAPDH* and then to transcript levels obtained from 3D collagen-only tumouroids. (ns = not significant, $p < 0.05$=*, $p < 0.01$=**, $p < 0.001$=***). ACM = artificial cancer mass; ECM = extracellular matrix; error bars = standard error of mean. (For interpretation of the references to colour in this figure legend, the reader is referred to the web version of this article.)

Please cite this article as: M. Pavlou, M. Shah, P. Gikas et al., Osteomimetic matrix components alter cell migration and drug response in a 3D tumour-engineered osteosarcoma model, Acta Biomaterialia, https://doi.org/10.1016/j.actbio.2019.07.011

Table 1
RT-PCR primers.

Gene	Forward Primer (5′ to 3′)	Reverse Primer (5′ to 3′)	size
PTEN	AATGTTCAGTGGCGGAACTTGC	CACACACAGGTAACGGCTGAGG	140
MMP9	TTCTGCCCGGACCAAGGATA	ACATAGGGTACATGAGCGCC	109
MCP1	TCAAACTGAAGCTCGCACTCT	CATTGATTGCATCTGGCTGAG	119
VEGFA	GTGAATGCAGACCAAAGAAAGA	CTCCAGGGCATTAGACAGCA	148
MCT4	CCACATCAAAGGGATCTTCTGC	CCATCCTCCATCCAGGGTTTT	100

3.4. Increased matrix complexity shifts osteosarcoma gene expression towards metabolic reprogramming

To further investigate the changes associated with increasing matrix complexity, the expression of selected genes that govern processes linked to osteosarcoma aggression [18] were assessed via real-time quantitative PCR (RT-qPCR) and correlated to morphological observations. Initially, the change in transcript levels of certain genes in response to culturing 143B and MG63 cells in 3D collagen instead of 2D monolayers was assessed. Indeed the difference was striking, as the expression of the gelatinase enzyme matrix metalloproteinase-9 (*MMP9*) increased by 37-fold ($p < 0.01$), vascular endothelial growth factor (*VEGF*) increased by 4.9-fold ($p < 0.0001$) and phosphatase and tensin homolog (*PTEN*) decreased by 0.5-fold ($p < 0.001$) in the highly metastatic 143B 3D cultures compared to monolayers (Fig. 3.H.). Culturing MG63 in 3D cultures increased *MMP9* by 2.4-fold ($p = 0.05$), *PTEN* by 1.6-fold ($p < 0.001$) and decreased *VEGF* by 0.57-fold ($p < 0.0001$) (Fig. 3.I.). Comparing the transcript levels of cells from the two different tumouroid compositions revealed greater changes for 143B tumouroids (Fig. 3.J.). Indeed, a 28-fold ($p < 0.05$) decrease in the *MMP-9* expression was measured in complex tumouroids. Furthermore, a 5-fold ($p < 0.01$) increase in expression of monocyte chemoattractant protein-1 (*MCP-1*) and a 1.2-fold ($p < 0.05$) increase of *PTEN* expression, which has an inverse relation to *MMP-9,* was also apparent when comparing complex to basic tumouroids. Although *VEGF* expression displayed no significant difference between complex and basic 143B tumouroids, there was a significant 1.8-fold ($p < 0.05$) increase in complex MG-63 tumouroids compared to basic (Fig. 3.K.). Both 143B and MG-63 complex tumouroids displayed a significant increase in monocarboxylate transporter 4 (*MCT-4*) expression, by 1.5-fold ($p < 0.05$) and 1.4-fold ($p < 0.05$), respectively.

3.5. Increasing matrix complexity alters drug response of osteosarcoma cells in 3D

Having confirmed that a complex environment, which replicates aspects of the bone intramedullary cavity, causes a shift towards an aggressive osteosarcoma phenotype in both tested cell lines, the effect of the commonly used anthracycline drug doxorubicin on 3D basic and complex tumouroids was tested. Doxorubicin is an antibiotic derived from *Streptomyces peucetius* [19], which has a mechanism of action involving DNA intercalation, blockage of DNA biosynthesis by stabilising the topoisomerase II complex thus preventing DNA replication [20] and increase of cytotoxicity by free-radical production [19]. Initially, to understand how the osteosarcoma cell lines behaved when exposed to doxorubicin, confluent 2D cultures of 143B and MG63 cells were exposed to 5 increasing drug concentrations (0.1–10 μM) for 24 h (Fig. 4.A-C.). Quantification of dsDNA indicated that there was significantly ($p < 0.0001$) more cell death in 143B than MG63 monolayers with respect to untreated cells (Fig. 4.B.). As doxorubicin intercalates in the DNA replication fork of dividing cells, 143B monolayer cultures may be more vulnerable to its effect as they replicate 3-times faster than MG-63 (Fig. 4.A.). Similarly, the PrestoBlue assay revealed a greater degree of metabolic change in 143B cells compared to MG63 for most tested concentrations of doxorubicin (Fig. 4.C.).

The next step was to test the hypothesis that complex tumouroids, which replicated the tumour microenvironment, would respond differently to doxorubicin and potentially more like that observed clinically. Cells in basic and complex ECM were cultured for 7 days and subsequently treated with 0.1, 1 and 10 μM doxorubicin hydrochloride for 24 h (Fig. 4.D-G.). Comparing the rate of cell death with respect to untreated tumouroids revealed that, although not statistically significant, 143B tumouroids in complex ECM were more resistant to drug treatment at concentrations 0.1 and 1 μM. Treatment with 10 μM doxorubicin lead to more cell death in complex 143B tumouroids (Fig. 4.D). As anticipated from the qPCR (Fig. 3.G.) and 2D drug assay (Fig. 4.B-C), the complex 143B tumouroids underwent a significantly ($p < 0.0001$) higher change in metabolic activity than basic tumouroids in response to doxorubicin (Fig. 4.E.). A similar observation was made for MG63 tumouroids as complex ECM composition resulted in a trending but not significant increase of metabolic activity after drug-treatment (Fig. 4.G.). Interestingly, the low-metastatic MG63 cells showed a trend, although not significant, resilience to doxorubicin-induced cell death when in the complex ECM (Fig. 4.F.).

4. Discussion

Herein, a geometrically compartmentalised 3D model of osteosarcoma was developed, which was composed of a core ACM and a surrounding acellular ECM compartment. Key material aspects were incorporated into the 3D model in the form of solid bone granules and bone-marrow matrix proteins to enable the investigation of cancer cell invasion patterns and drug responses in a biologically relevant environment.

The application of 3D models in cancer research has grown in the last two decades [21,22], with promising approaches being borrowed from tissue engineering [23–26] to provide *in vitro* models with both biological relevance and high-throughput potential for drug-screening; e.g. 3D tumour spheroids [27] and the hanging-drop method [28]. Several of these approaches have cast new light on basic cancer biology and re-emphasised how the tumour microenvironment dictates cancer fate [29,30]. As the field progresses for most epithelial cancers, rare cancers such as osteosarcoma have been marginalised in terms of novel drug discovery and preclinical model development. Indeed, although *in vitro* osteosarcoma models have been reported and reviewed for their relevance to the disease *in vivo* [31], most models are either scaffold-free, to provide flexibility, or are scaffold-based to provide the 3D structure – none combine both. The geometrically compartmentalised tumouroids described herein combine flexibility and 3D structure. This provides the opportunity to study how the matrix component of the stroma, which was developed to reproduce the physical niche in bone, changes cancer invasion and drug response.

Collagen type I is the most prevalent ECM protein in bone and its increased expression and linearised fibrils have been associated

with cancer progression [32]. It has been shown *in vitro* that invasive cancer cells have a higher affinity for matrices expressing the collagen type I peptide motif GFOGER (where O = hydroxyproline) and laminin-111 motif IKVAV [33], the components of our basic tumouroid cultures. Collagen-based hydrogels have a restricted stiffness range which can limit applications for preclinical osteosarcoma research [34,35]. Through the use of the compression technique collagen hydrogels were generated with an average

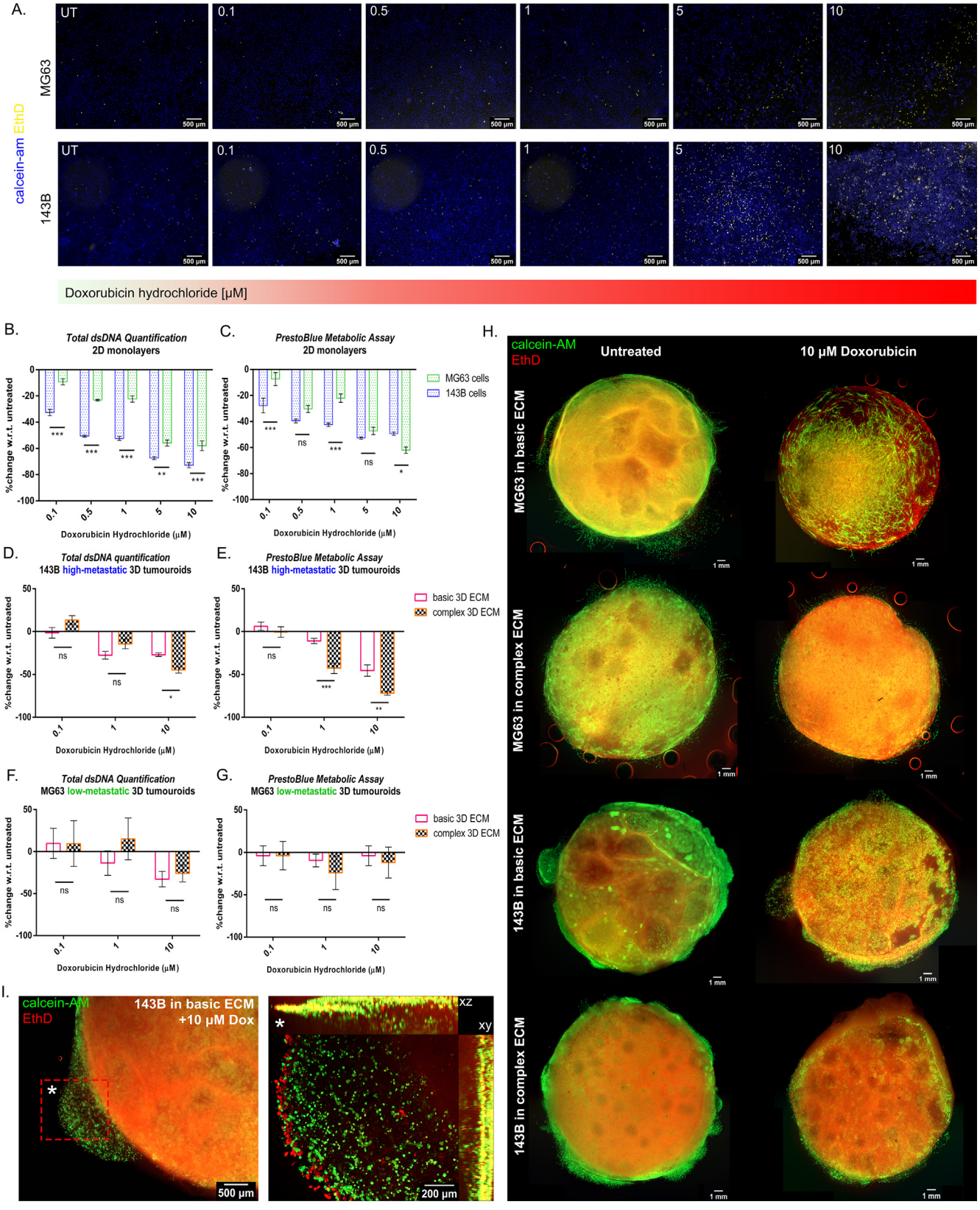

Please cite this article as: M. Pavlou, M. Shah, P. Gikas et al., Osteomimetic matrix components alter cell migration and drug response in a 3D tumour-engineered osteosarcoma model, Acta Biomaterialia, https://doi.org/10.1016/j.actbio.2019.07.011

break force of 0.216 Newtons [36] and a mean tensile break strength of 0.6 ± 0.11 MPa with modulus of 1.5 ± 0.36 MPa [37], along with an ~48-fold increase in protein density to 120 mg/ml [38]. Although this may not approximate the physiological properties of bone, the plastic compression method has been shown to promote cell proliferation and migration, which is expected of stiff matrices [39]. Bone with osteosarcoma, like its healthy counterpart, undergoes constant remodelling and dynamic homeostasis during which transformed osteoblasts/MSCs deposit pre-mineralised osteoid composed of 95% collagen type I. As such, it was considered an appropriate baseline substrate for priming physiological osteosarcoma behaviour.

A specific organisation of cells in 3D and distinct migration patterns were recorded in tumouroids. High-metastatic 143B tumouroids with basic matrix composition (collagen I + laminin) formed cell clusters in the ACM by day 2 and then invaded the surrounding acellular ECM by day 5 of culture, predominantly as cell sheets (Fig. 2.C.). The equivalent low-metastatic MG63 tumouroids exhibited similar behaviour. Previous work on collective sheet-like migration described this as a modular control system; boundary cells are converted into pioneers while the rest of the cells trace and follow the pattern of pioneers through cell-cell coordination in a growth-factor independent manner [40].

Both 143B and MG63 tumouroids exhibited another collective cell migration pattern in the form of 3D invasive bodies with a spheroid-like morphology. These irregular spheroids grew either attached to the ACM or detached and migrated into the surrounding acellular ECM (Fig. 2.D.). High-metastatic 143B tumouroids produced significantly larger spheroids compared to the low-metastatic MG63 cultures (Fig. 2.G.). This was apportioned to the 3-fold higher proliferation rate (Fig. 2.H.) and the high metastatic potential of 143B cells [18]. The generation of spheroids may also be key when evaluating patient-derived osteosarcoma tumouroids since a similar pattern of cell migration in colorectal cancer reportedly acted as an independent indicator of distant metastases and poor survival [41]. It is important to highlight that although other hallmarks of cancer are missing from this model, the introduction of a biomimetic matrix in 3D *in vitro* was sufficient to induce phenotypes that are linked to *in vivo*.

Within the complex osteosarcoma model described herein, the material properties of the biomimetic 'bone' compartment containing collagen, cancer cells and NuOss® bone granules are different to the biomimetic 'bone marrow' component that is the collagen-laminin-fibronectin surround. Indeed, the addition of NuOss® bone granules most likely made the ACM stiffer. Although outside of the remit of this study, it is interesting to note that invasion of both the 143B and MG63 cells in 3D, at least in terms of sheet invasion, was significantly greater when NuOss® granules were introduced to the ACM (Supp. Fig. 3.A-E.). The vast majority of studies have described the phenomenon of durotaxis, where cells move to the stiffest part of 3D gels [42]. In stark contrast to this, the current study reveals that osteosarcoma cell invasion is significantly enhanced (Fig. 3.C-E.) where a reverse stiffness gradient exists, in that cells embedded in a stiff 'bone-like' matrix, invade faster into a 'softer' surrounding matrix. This likely confirms that the observations made in the current study are indeed invasion, as opposed to cell migration, and that invasive pathways are playing a significant role in the morphology of invasion (Fig. 3.B & 3.G.), as well as the rate (Fig. 3.C-E.).

The plasticity of osteosarcoma cells in response to changes in their surrounding matrix was recorded both morphologically, in terms of the invasion profile, and molecularly via qPCR. Matrix supplementation with NuOss® bone granules led to increased invasive bodies in high-metastatic 143B tumouroids (Fig. 3.D.) and appeared to hinder their migration into the surrounding ECM (Fig. 3.E.). This was also reflected by low *MMP-9* expression (Fig. 3.J.). Although osteosarcoma *in vivo* has been associated with high levels of MMP [43–46], cancer growth and invasion within this 3D model could be portrayed by a switch to protease-independent collective cell migration [47]. Low *MMP-9* levels could also have been the result of high *PTEN* expression in complex 143B tumouroids (Fig. 3.J.), since *PTEN* expression hinders *MMP-9* promoter activity via TNFα [48]. In the context of osteosarcoma, *PTEN* inhibits tumour-induced osteoclast differentiation to counteract bone resorption [49]. As such, *PTEN* upregulation in complex 143B tumouroids containing NuOss® bone granules would be an expected result of the elevated levels of *MCP-1* (Fig. 3.J.). *MCP-1* is an early stress response signal [50] which in osteosarcoma triggers osteoclastogenesis from monocytes and attracts osteoclasts to the cancer site in order to resorb the surrounding bone [51]. This is in agreement with previous reports that 143B cells can produce osteolytic tumours *in vivo* [52] due to the inherent malignancy profile of the immortalised cell line [51]. The addition of NuOss® caused 143B tumouroids to upregulate *MCT-4* (Fig. 3.J.), suggesting that the cancer cells shifted towards a glycolytic metabolism which is linked to poor cancer patient survival [53]. As gate-keeper of lactate efflux, *MCT-4* upregulation could also reflect the *in vivo* phenomenon of transformed MSCs promoting osteosarcoma migration via lactate [54]. This is however an observation based on the expression of a single gene of the glycolytic switch and more extensive molecular analysis would be required to fully elucidate matrix induced metabolic reprogramming. It should be noted that on the whole a divergent gene expression profile was observed when comparing MG63 to 143B cells, which has been documented before [55], and is likely to reflect the differences in osteosarcoma characteristics. Indeed, as we specifically chose genes linked to metastasis, this further confirms that the complex tumouroid is likely to be facilitating the cells natural capacity for metastasis.

The 3D tumouroids described herein were created to interrogate the effects of a biomimetic matrix on osteosarcoma behaviour. A limitation of these models is the lack other key elements of the tumour microenvironment such as neovascularisation and interac-

Fig. 4. Analysis of cell sensitivity to doxorubicin treatment in basic and complex tumouroids. A. Panel of live/dead fluorescence images of 2D 143B and MG63 monolayers treated for 24 h with increasing doxorubicin concentrations. B. Quantitative assessment of cell death rate in 2D monolayers of 143B and MG63 cells after 24 h treatment with increasing doxorubicin concentrations, using dsDNA quantification. C. Quantitative assessment of metabolic change rate in 2D monolayers of 143B and MG63 cells after 24 h treatment with increasing doxorubicin concentrations, using PrestoBlue metabolic assay. D. Quantitative assessment of cell death rate in 3D 143B tumouroids with basic or complex ECM after 24 h treatment with increasing doxorubicin concentrations, using dsDNA quantification. E. Quantitative assessment of metabolic change rate in 3D 143B tumouroids with basic or complex ECM after 24 h treatment with increasing doxorubicin concentrations, using PrestoBlue metabolic assay. F. Quantitative assessment of cell death rate in 3D MG63 tumouroids with basic or complex ECM after 24 h treatment with increasing doxorubicin concentrations, using dsDNA quantification. G. Quantitative assessment of metabolic change rate in 3D MG63 tumouroids with basic or complex ECM after 24 h treatment with increasing doxorubicin concentrations, using PrestoBlue metabolic assay. H. Birdseye view of MG63 and 143B tumouroids with basic and complex ECM. Tumouroids were incubated for 7 days and treated with doxorubicin for 24 h. These are collages of single live/dead fluorescence images of the ACM compartment of tumouroids in order to provide a visual representation of cell death and doxorubicin penetrance in the 3D cancer masses. I. Live/dead stained image of the lower left ACM quadrant of a 143B tumouroid in basic ECM after treatment with 10 μM doxorubicin. Invasive spheroid body is asterisk-marked and magnified to emphasise the cell death occurring mostly on the periphery. ACM = artificial cancer mass; ECM = extracellular matrix; error bars = standard error of mean.

Please cite this article as: M. Pavlou, M. Shah, P. Gikas et al., Osteomimetic matrix components alter cell migration and drug response in a 3D tumour-engineered osteosarcoma model, Acta Biomaterialia, https://doi.org/10.1016/j.actbio.2019.07.011

tion with other cell types. Nevertheless, given the diversity between pioneer cancer cells and follower cells within a metastasising tumour *in vivo*, obtaining analogous morphological and molecular diversity within tumouroids illustrates an improved biological relevance.

To test the capacity of tumouroids as a drug screening platform we exposed complex and basic high metastatic 143B tumouroids to doxorubicin after an initial 7 day culture period. It was hypothesised that osteosarcoma cells cultured in the complex 3D matrix would infer a distinct drug response compared to cells within a basic matrix. To experimentally test this hypothesis, day 7 tumouroids were exposed to 0.1–10 μM doxorubicin hydrochloride for 24 h. This corresponds to 50–5000 ng/ml doxorubicin, which includes the range of plasma C_{max} (39.8 ± 15.3 to 630.4 ± 22.1 ng/ml) achieved in individuals with normal body surface area (BSA) after a 24 h infusion [56].

Analysis of the doxorubicin treated tumouroids revealed 143B cells grown in the complex matrix composition underwent a greater rate of change in metabolic activity than basic tumouroids in response to doxorubicin (Fig. 4.E.) whereas MG63 complex tumouroids only trended to an increased rate of metabolic change at 1 μM (Fig. 4.G.). Furthermore, the complex ECM composition conferred a trend for resistance to drug-induced death in both cell lines compared to the basic ECM counterparts (Fig. 4.D. & 4.F.). At the highest drug dose, 143B complex tumouroids had a greater rate in cell death, which may indicate the requirement for higher drug doses or more efficient doxorubicin-like drugs clinically. 143B cells have already been shown to generate drug-resistant tumours *in vivo* [57,58], confirming that complex 3D tumouroids are capable of reproducing aspects of cancer cell behaviour *in vitro*. Qualitative observations of live-dead stained tumouroids with basic and complex ECM composition indicated that the majority of cell death existed in the periphery of the ACM (Fig. 4.H.) and invasive bodies (Fig. 4.I.). Following the paradigm of a protective cancer core and limited drug penetrance *in vivo*, this observation is not surprising. The cells at the periphery are exposed to the drug for longer time periods hence are more susceptible to cell death.

5. Conclusions

The potential mechanisms through which osteosarcoma achieves chemoresistance have been reviewed extensively [59], concluding that both the intrinsic cellular profile and the extracellular environment impact cancer cell behaviour. To our knowledge, the complex osteosarcoma tumouroids described herein are the first geometrically modular 3D cultures to incorporate matrix components of the osteosarcoma niche, and capture the adaptive nature of tumour cells in response to changes in their surroundings and drug treatment. It is envisaged that this body of work will engage the field and generate the impetus for further development of biomimetic osteosarcoma models.

Acknowledgements

This work was funded by Bone Cancer Research Trust (BCRT/40/14) and SCAT Bone Cancer Trust (SCAT/OsM). We would also like to acknowledge the RNOH charity.

Declaration of Competing Interest

The authors declare no conflict of interests.

Appendix A. Supplementary data

Supplementary data to this article can be found online at https://doi.org/10.1016/j.actbio.2019.07.011.

References

[1] G. Ottaviani, N. Jaffe, The epidemiology of osteosarcoma, Cancer Treat. Res. 152 (2009) 3–13.
[2] A. Abarrategi, J. Tornin, L. Martinez-Cruzado, A. Hamilton, E. Martinez-Campos, J.P. Rodrigo, M.V. González, N. Baldini, J. Garcia-Castro, R. Rodriguez, Osteosarcoma: cells-of-origin, cancer stem cells, and targeted therapies, Stem Cells Int. 2016 (2016) 3631764.
[3] P. Zioupos, J.D. Currey, Changes in the stiffness, strength, and toughness of human cortical bone with age, Bone 22 (1) (1998) 57–66.
[4] X.-D. Chen, V. Dusevich, J.Q. Feng, S.C. Manolagas, R.L. Jilka, Extracellular matrix made by bone marrow cells facilitates expansion of marrow-derived mesenchymal progenitor cells and prevents their differentiation into osteoblasts, J. Bone Mineral Res. 22 (12) (2007) 1943–1956.
[5] L.E. Jansen, N.P. Birch, J.D. Schiffman, A.J. Crosby, S.R. Peyton, Mechanics of intact bone marrow, J. Mech. Behav. Biomed. Mater. 50 (2015) 299–307.
[6] J.H. Ahn, W.H. Cho, J.A. Lee, D.H. Kim, J.H. Seo, J.S. Lim, Bone mineral density change during adjuvant chemotherapy in pediatric osteosarcoma, Ann. Pediatric Endocrinol. Metabol. 20 (3) (2015) 150–154.
[7] E. Ruza, L. Sierrasesumaga, C. Azcona, A. Patino-Garcia, Bone mineral density and bone metabolism in children treated for bone sarcomas, Pediatr. Res. 59 (6) (2006) 866–871.
[8] P. Clezardin, C.M. Serre, M.C. Trzeciak, J. Drouin, P.D. Delmas, Thrombospondin binds to the surface of human osteosarcoma cells and mediates platelet-osteosarcoma cell interaction, Cancer Res. 51 (10) (1991) 2621–2627.
[9] C. Voland, C.M. Serre, P. Delmas, P. Clezardin, Platelet-osteosarcoma cell interaction is mediated through a specific fibrinogen-binding sequence located within the N-terminal domain of thrombospondin 1, J. Bone Miner. Res. 15 (2) (2000) 361–368.
[10] S. Takagi, A. Takemoto, M. Takami, T. Oh-Hara, N. Fujita, Platelets promote osteosarcoma cell growth through activation of the platelet-derived growth factor receptor-Akt signaling axis, Cancer Sci. 105 (8) (2014) 983–988.
[11] D.J. Scholten 2nd, C.M. Timmer, J.D. Peacock, D.W. Pelle, B.O. Williams, M.R. Steensma, Down regulation of Wnt signaling mitigates hypoxia-induced chemoresistance in human osteosarcoma cells, PLoS ONE 9 (10) (2014) e111431.
[12] L. Roncuzzi, F. Pancotti, N. Baldini, Involvement of HIF-1alpha activation in the doxorubicin resistance of human osteosarcoma cells, Oncol. Rep. 32 (1) (2014) 389–394.
[13] A. Marion, F.X. Dieudonne, A. Patino-Garcia, F. Lecanda, P.J. Marie, D. Modrowski, Calpain-6 is an endothelin-1 signaling dependent protective factor in chemoresistant osteosarcoma, International journal of cancer, J. Int. Cancer 130 (11) (2012) 2514–2525.
[14] Y. Suzuki, Y. Nishida, T. Naruse, T. Gemba, N. Ishiguro, Pericellular matrix formation alters the efficiency of intracellular uptake of oligonucleotides in osteosarcoma cells, J. Surg. Res. 152 (1) (2009) 148–156.
[15] Y. Chen, M. Sonnaert, S.J. Roberts, F.P. Luyten, J. Schrooten, Validation of a PicoGreen-based DNA quantification integrated in an RNA extraction method for two-dimensional and three-dimensional cell cultures, Tissue Eng. Part C, Methods 18 (6) (2012) 444–452.
[16] S.A. Bustin, V. Benes, J.A. Garson, J. Hellemans, J. Huggett, M. Kubista, R. Mueller, T. Nolan, M.W. Pfaffl, G.L. Shipley, J. Vandesompele, C.T. Wittwer, The MIQE guidelines: minimum information for publication of quantitative real-time PCR experiments, Clin. Chem. 55 (4) (2009) 611–622.
[17] S. Lemma, S. Avnet, M. Salerno, T. Chano, N. Baldini, Identification and validation of housekeeping genes for gene expression analysis of cancer stem cells, PLoS ONE 11 (2) (2016) e0149481.
[18] A.B. Mohseny, I. Machado, Y. Cai, K.L. Schaefer, M. Serra, P.C. Hogendoorn, A. Llombart-Bosch, A.M. Cleton-Jansen, Functional characterization of osteosarcoma cell lines provides representative models to study the human disease, Laboratory Investigation 91 (8) (2011) 1195–1205.
[19] E. Ravina, Anthracyclines, The Evolution of Drug Discovery: From Traditional Medicines to Modern Drugs, John Wiley & Sons, 2011, p. 291.
[20] Y. Pommier, E. Leo, H. Zhang, C. Marchand, DNA topoisomerases and their poisoning by anticancer and antibacterial drugs, Chem. Biol. 17 (5) (2010) 421–433.
[21] F. Pampaloni, E.G. Reynaud, E.H. Stelzer, The third dimension bridges the gap between cell culture and live tissue, Nat. Rev. Mol. Cell Biol. 8 (10) (2007) 839–845.
[22] C. Wang, Z. Tang, Y. Zhao, R. Yao, L. Li, W. Sun, Three-dimensional in vitro cancer models: a short review, Biofabrication 6 (2) (2014) 022001.
[23] A. Nyga, U. Cheema, M. Loizidou, 3D tumour models: novel in vitro approaches to cancer studies, J. Cell Commun. Signaling 5 (3) (2011) 239–248.
[24] M.R. Carvalho, D. Lima, R.L. Reis, V.M. Correlo, J.M. Oliveira, Evaluating biomaterial- and microfluidic-based 3D tumor models, Trends Biotechnol. 33 (11) (2015) 667–678.

[25] M.R. Carvalho, D. Lima, R.L. Reis, J.M. Oliveira, V.M. Correlo, Anti-cancer drug validation: the contribution of tissue engineered models, Stem Cell Rev. 13 (3) (2017) 347–363.
[26] K. Klimkiewicz, K. Weglarczyk, G. Collet, M. Paprocka, A. Guichard, M. Sarna, A. Jozkowicz, J. Dulak, T. Sarna, C. Grillon, C. Kieda, A 3D model of tumour angiogenic microenvironment to monitor hypoxia effects on cell interactions and cancer stem cell selection, Cancer Lett. 396 (2017) 10–20.
[27] E.C. Costa, A.F. Moreira, D. de Melo-Diogo, V.M. Gaspar, M.P. Carvalho, I.J. Correia, 3D tumor spheroids: an overview on the tools and techniques used for their analysis, Biotechnol. Adv. 34 (8) (2016) 1427–1441.
[28] M. Rimann, S. Laternser, A. Gvozdenovic, R. Muff, B. Fuchs, J.M. Kelm, U. Graf-Hausner, An in vitro osteosarcoma 3D microtissue model for drug development, J. Biotechnol. 189 (2014) 129–135.
[29] K. Pietras, A. Ostman, Hallmarks of cancer: interactions with the tumor stroma, Exp. Cell Res. 316 (8) (2010) 1324–1331.
[30] D. Hanahan, R.A. Weinberg, Hallmarks of cancer: the next generation, Cell 144 (5) (2011) 646–674.
[31] A. De Luca, L. Raimondi, F. Salamanna, V. Carina, V. Costa, D. Bellavia, R. Alessandro, M. Fini, G. Giavaresi, Relevance of 3d culture systems to study osteosarcoma environment, J. Exp. Clin. Cancer Res. 37 (1) (2018) 2.
[32] M. Egeblad, M.G. Rasch, V.M. Weaver, Dynamic interplay between the collagen scaffold and tumor evolution, Curr. Opin. Cell Biol. 22 (5) (2010) 697–706.
[33] A.V. Taubenberger, L.J. Bray, B. Haller, A. Shaposhnykov, M. Binner, U. Freudenberg, J. Guck, C. Werner, 3D extracellular matrix interactions modulate tumour cell growth, invasion and angiogenesis in engineered tumour microenvironments, Acta Biomater. 36 (2016) 73–85.
[34] E. Mylona, Z.H. Dailiana, X. Trepat, M.G. Lagoudakis, Substrate rigidity dictates phenotype, survival, and mechanics of primary human osteosarcoma cells, Eur. Symp. Biomed. Eng. (2008) 1–4.
[35] H.Y. Yoshikawa, J. Cui, K. Kratz, T. Matsuzaki, S. Nakabayashi, A. Marx, U. Engel, A. Lendlein, M. Tanaka, Quantitative evaluation of adhesion of osteosarcoma cells to hydrophobic polymer substrate with tunable elasticity, J. Phys. Chem. B 116 (28) (2012) 8024–8030.
[36] I. Massie, A.K. Kureshi, S. Schrader, A.J. Shortt, J.T. Daniels, Optimization of optical and mechanical properties of real architecture for 3-dimensional tissue equivalents: towards treatment of limbal epithelial stem cell deficiency, Acta Biomater. 24 (2015) 241–250.
[37] R.A. Brown, M. Wiseman, C.B. Chuo, U. Cheema, S.N. Nazhat, Ultrarapid engineering of biomimetic materials and tissues: fabrication of nano- and microstructures by plastic compression, Adv. Funct. Mater. 15 (11) (2005) 1762–1770.
[38] T. Magdeldin, V. Lopez-Davila, J. Pape, G.W. Cameron, M. Emberton, M. Loizidou, U. Cheema, Engineering a vascularised 3D in vitro model of cancer progression, Sci. Rep. 7 (2017) 44045.
[39] U. Cheema, R.A. Brown, Rapid fabrication of living tissue models by collagen plastic compression: understanding three-dimensional cell matrix repair in vitro, Adv. Wound Care 2 (4) (2013) 176–184.
[40] P. Vitorino, T. Meyer, Modular control of endothelial sheet migration, Genes Dev. 22 (23) (2008) 3268–3281.
[41] K. Tamura, S. Yokoyama, J. Ieda, K. Takifuji, T. Hotta, K. Matsuda, Y. Oku, T. Watanabe, T. Nasu, S. Kiriyama, N. Yamamoto, Y. Nakamura, J.E. Shively, H. Yamaue, Hollow spheroids beyond the invasive margin indicate the malignant potential of colorectal cancer, BMJ Open 1 (1) (2011).
[42] E. Hadjipanayi, V. Mudera, R.A. Brown, Guiding cell migration in 3D: A collagen matrix with graded directional stiffness, Cell Motility 66 (3) (2009) 121–128.
[43] K. Bjornland, K. Flatmark, S. Pettersen, A.O. Aaasen, O. Fodstad, G.M. Maelandsmo, Matrix metalloproteinases participate in osteosarcoma invasion, J. Surg. Res. 127 (2) (2005) 151–156.
[44] S. Ferrari, F. Bertoni, L. Zanella, E. Setola, P. Bacchini, M. Alberghini, M. Versari, G. Bacci, Evaluation of P-glycoprotein, HER-2/ErbB-2, p53, and Bcl-2 in primary tumor and metachronous lung metastases in patients with high-grade osteosarcoma, Cancer 100 (9) (2004) 1936–1942.
[45] J.T. Korpi, J. Hagstrom, N. Lehtonen, J. Parkkinen, T. Sorsa, T. Salo, M. Laitinen, Expression of matrix metalloproteinases-2, -8, -13, -26, and tissue inhibitors of metalloproteinase-1 in human osteosarcoma, Surg. Oncol. 20 (1) (2011) e18–e22.
[46] C.C. Lynch, Matrix metalloproteinases as master regulators of the vicious cycle of bone metastasis, Bone 48 (1) (2011) 44–53.
[47] P. Friedl, D. Gilmour, Collective cell migration in morphogenesis, regeneration and cancer, Nat. Rev. Mol. Cell Biol. 10 (7) (2009) 445–457.
[48] S.K. Moon, H.M. Kim, C.H. Kim, PTEN induces G1 cell cycle arrest and inhibits MMP-9 expression via the regulation of NF-kappaB and AP-1 in vascular smooth muscle cells, Arch. Biochem. Biophys. 421 (2) (2004) 267–276.
[49] Y. Xi, Y. Chen, PTEN plays dual roles as a tumor suppressor in osteosarcoma cells, J. Cell. Biochem. 118 (9) (2017) 2684–2692.
[50] P. Rahimi, C.Y. Wang, P. Stashenko, S.K. Lee, J.A. Lorenzo, D.T. Graves, Monocyte chemoattractant protein-1 expression and monocyte recruitment in osseous inflammation in the mouse, Endocrinology 136 (6) (1995) 2752–2759.
[51] T. Ohba, H.A. Cole, J.M. Cates, D.A. Slosky, H. Haro, T. Ando, H.S. Schwartz, J.G. Schoenecker, Bisphosphonates inhibit osteosarcoma-mediated osteolysis via attenuation of tumor expression of MCP-1 and RANKL, J. Bone Mineral Res. 29 (6) (2014) 1431–1445.
[52] J. Yuan, C. Ossendorf, J.P. Szatkowski, J.T. Bronk, A. Maran, M. Yaszemski, M.E. Bolander, G. Sarkar, B. Fuchs, Osteoblastic and osteolytic human osteosarcomas can be studied with a new xenograft mouse model producing spontaneous metastases, Cancer Invest. 27 (4) (2009) 435–442.
[53] J. Pérez-Escuredo, V.F. Van Hée, M. Sboarina, J. Falces, V.L. Payen, L. Pellerin, P. Sonveaux, Monocarboxylate transporters in the brain and in cancer, Biochim. Biophys. Acta (BBA) – Mol. Cell Res. 1863 (10) (2016) 2481–2497.
[54] G. Bonuccelli, S. Avnet, G. Grisendi, M. Salerno, D. Granchi, M. Dominici, K. Kusuzaki, N. Baldini, Role of mesenchymal stem cells in osteosarcoma and metabolic reprogramming of tumor cells, Oncotarget 5 (17) (2014) 7575–7588.
[55] L. Ren, A. Mendoza, J. Zhu, J.W. Briggs, C. Halsey, E.S. Hong, S.S. Burkett, J. Morrow, M.M. Lizardo, T. Osborne, S.Q. Li, H.H. Luu, P. Meltzer, C. Khanna, Characterization of the metastatic phenotype of a panel of established osteosarcoma cells, Oncotarget 6 (30) (2015) 29469–29481.
[56] D.R. Barpe, D.D. Rosa, P.E. Froehlich, Pharmacokinetic evaluation of doxorubicin plasma levels in normal and overweight patients with breast cancer and simulation of dose adjustment by different indexes of body mass, Eur. J. Pharm. Sci. 41 (3) (2010) 458–463.
[57] P. Hingorani, W. Zhang, R. Gorlick, E.A. Kolb, Inhibition of Src phosphorylation alters metastatic potential of osteosarcoma in vitro but not in vivo, Clin. Cancer Res. 15 (10) (2009) 3416.
[58] P. Brennecke, M.J. Arlt, C. Campanile, K. Husmann, A. Gvozdenovic, T. Apuzzo, M. Thelen, W. Born, B. Fuchs, CXCR4 antibody treatment suppresses metastatic spread to the lung of intratibial human osteosarcoma xenografts in mice, Clin. Exp. Metastasis 31 (3) (2014) 339–349.
[59] H. He, J. Ni, J. Huang, Molecular mechanisms of chemoresistance in osteosarcoma (Review), Oncol. Lett. 7 (5) (2014) 1352–1362.

Please cite this article as: M. Pavlou, M. Shah, P. Gikas et al., Osteomimetic matrix components alter cell migration and drug response in a 3D tumour-engineered osteosarcoma model, Acta Biomaterialia, https://doi.org/10.1016/j.actbio.2019.07.011